Inorganic Chemistry

Article

pubs.acs.org/IC

Synthesis and Spectroscopy of New Plutonium(III) and -(IV) Molybdates: Comparisons of Electronic Characteristics

Justin N. Cross, Samantha K. Cary, Jared T. Stritzinger, Matthew J. Polinski, and Thomas E. Albrecht Schmitt*

Department of Chemistry and Biochemistry, Florida State University, 95 Chieftan Way, 310 DLC, Tallahassee, Florida 32306-4390, United States

Supporting Information

ABSTRACT: Synthesis of a plutonium(III) molybdate bromide, $PuMoO_4Br(H_2O)$, has been accomplished using hydrothermal techniques in an inert-atmosphere glovebox. The compound is green in color, which is in stark contrast to the typical blue color of plutonium(III) complexes. The unusual color arises from the broad charge transfer (CT) spanning from approximately 300 to 500 nm in the UV−vis−near-IR spectra. Repeating the synthesis with an increase in the reaction temperature results in the formation of a plutonium(IV) molybdate, $Pu_3Mo_6O_{24}(H_2O)_2$, which also has a broad CT band and red-shifted f−f transitions. Performing an analogous reaction with neodymium produced a completely different product, $[Nd(H_2O)_3][NdMo_{12}O_{42}]\cdot 2H_2O$, which is built of Silverton-type polyoxometallate clusters.

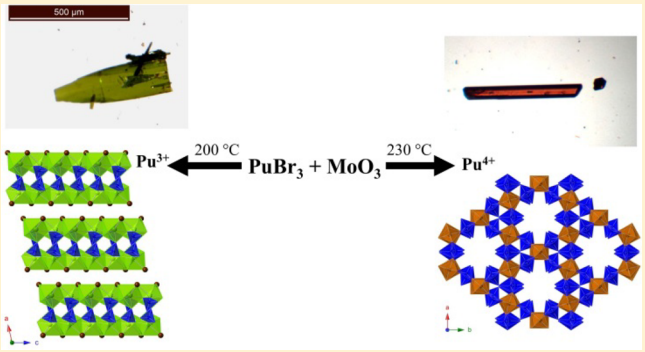

INTRODUCTION

The electronic character of actinide complexes has been a rich research area because these elements behave unlike any other group in the periodic table. They generally retain the spectroscopic and magnetic properties associated with the number of f electrons regardless of the coordination environment but can still form partially covalent bonds because of symmetry and energy matching of the 5f and 6d orbitals.[1] This partially covalent interaction can lead to a discontinuity between low-valent actinides and their lanthanide congeners either through shorter bond lengths, different structures, or differences in the electronic character.[2] This discontinuity is not always observed, and the expression of covalent effects depends greatly on the nature of the ligand. The more ionic ligands such as aquotriflates, phosphonates, and phosphites generate very similar 4f and 5f compounds.[3] Conversely, softer, more polarizable ligands, such as borate, imidodiphosphinochalcogenides, and cyclic π donors, show differences between the lanthanides and actinides.

We have recently explored the reactions of oxyanions with high hyperpolarizabilities and the actinides to probe this discontinuity because we believe that there is a direct relationship between the hyperpolarizability of a single M−O bond and the polarizability of the entire oxyanion.[4] These ligands have strong second-order Jahn−Teller distortions such as tellurite, tungstate, or molybdate. The ability of these ligands to adopt multiple geometries and polymerize, forming more polarizable anions, makes them attractive candidates for this work. We have reported the synthesis of plutonium(IV) tellurites and molybdates. The hydrothermal reaction of $PuCl_3$ and TeO_2 produces a compound isotypic to that of cerium(IV). When sulfate is introduced to the reaction mixture, there is a distinct difference in products because cerium(III) remains trivalent while plutonium(III) oxidizes to plutonium(IV).[5] The reaction of $PuCl_3$, MoO_3, and Cs_2CO_3 produces a plutonium(IV) complex that is structurally similar to the cerium(IV) complex but has partially reduced molybdate and incorporates Cs^+, whereas the molybdate in the cerium(IV) version is fully oxidized and there is no Cs^+.[6] In a continuation of this work, we have produced two new plutonium molybdates with unusual absorption spectra.

The hydrothermal reaction of a $PuBr_3$ residue and MoO_3 at 200 °C in an argon-filled glovebox produces green crystals of the plutonium(III) complex $PuMoO_4Br(H_2O)$ (**$Pu^{III}Mo$**). Repeating the reaction at 230 °C produced orange crystals of the plutonium(IV) complex $Pu_3Mo_6O_{24}(H_2O)_2$ (**$Pu^{IV}Mo$**). A reaction with $NdBr_3$ and MoO_3 at 200 °C did not produce a structure isotypic to **$Pu^{III}Mo$** but $[Nd(H_2O)_3][NdMo_{12}O_{42}]\cdot 2H_2O$ (**$Nd^{III}Mo$**) instead.

EXPERIMENTAL SECTION

Syntheses. MoO_3 (99.9995% Alfa Aesar) and $NdBr_3\cdot XH_2O$ (hydrobromic acid; ACS reagent 48%, Sigma Aldrich) were used as obtained. Weapons-grade plutonium (94% ^{239}Pu, 6% ^{240}Pu) in the form of $PuCl_3$ was received from LANL. Because it had oxidized to red

Received: December 20, 2013
Published: March 6, 2014

   dx.doi.org/10.1021/ic403116r | Inorg. Chem. 2014, 53, 3148−3152

$PuOCl_2$, reduction back to plutonium(III) was accomplished by adding 50 μL of concentrated HBr and reducing to a residue in a 130 °C box furnace. The residue was then used as the starting plutonium source. Reactions were run in a Parr 4749 autoclave with a 10-mL-internal-volume poly(tetrafluoroethylene) (PTFE) liner for plutonium and a 23-mL-internal-volume liner for neodymium. Deionized water was used in all reactions. ***Caution!*** *^{239}Pu ($t_{1/2}$ = 24065 years) and ^{240}Pu ($t_{1/2}$ = 6537 years) represent serious health risks owing to their α and γ emission. All studies with plutonium were conducted in a laboratory dedicated to studies on transuranium elements. This laboratory is located in a nuclear science facility and is equipped with HEPA-filtered hoods and negative-pressure gloveboxes that are ported directly into the hoods. A series of counters continually monitor the radiation levels in the laboratory. The laboratory is licensed by the Nuclear Regulatory Commission. All experiments were carried out with approved safety operating procedures. All free-flowing solids are worked within gloveboxes, and products are only examined when coated with either water or immersion oil and water. There are significant limitations in accurately determining yield with plutonium compounds because this requires drying, isolating, and weighing a solid, which poses certain risks, as well as manipulation difficulties given the small quantities employed in the reactions.*

*$PuMoO_4Br(H_2O)$ (**$Pu^{III}Mo$**).* $PuOCl_2$ (0.0102 g, 0.0311 mmol) and concentrated HBr (50 μL) were heated in a 10 mL Teflon liner at 130 °C until reduced to a solid residue. After cooling to room temperature, the liner was moved to an argon-filled glovebox. MoO_3 (0.0045 g, 0.0308 mmol) and 200 μL of argon-sparged deionized water were added to the liner. The liner was sealed in a steel jacket, heated to 200 °C in a box furnace in the glovebox for 3 days, and then slow-cooled over 2 days. The resulting product was rinsed with deionized water, and bright-green plates were isolated.

*$Pu_3Mo_6O_{24}(H_2O)_2$ (**$Pu^{IV}Mo$**).* $PuOCl_2$ (0.0106 g, 0.0323 mmol) and concentrated HBr (50 μL) were heated in a 10 mL Teflon liner at 130 °C until reduced to a solid residue. After cooling to room temperature, the liner was moved to an argon-filled glovebox. MoO_3 (0.0050 g, 0.0343 mmol) and 200 μL of argon-sparged deionized water were added to the liner. The liner was sealed in a steel jacket, heated to 230 °C in a box furnace in the glovebox for 3 days, and then slow-cooled over 2 days. The resulting product was rinsed with deionized water, and orange columns were isolated.

*$[Nd(H_2O)_3][NdMo_{12}O_{42}]\cdot 2H_2O$ (**$Nd^{III}Mo$**).* $NdBr_3\cdot XH_2O$ (0.102 g, 0.200 mmol), MoO_3 (0.0288 g, 0.200 mmol), and 2 mL of deionized water were added to a 23 mL PTFE liner. The liner was sealed in a steel autoclave, heated to 200 °C for 3 days, and then slow-cooled over 2 days. Pink cubes of **$Nd^{III}Mo$** were isolated along with pink fibers, of which no suitable crystals for single-crytal X-ray diffraction could be isolated.

Crystallographic Studies. Single crystals of **$Pu^{III}Mo$**, **$Pu^{IV}Mo$**, and **$Nd^{III}Mo$** were mounted on cryoloops with viscous immersion oil and optically aligned on a Bruker APEXII Quest or Quazar X-ray diffractometer using a digital camera. Initial intensity measurements were performed using a IμS X-ray source (Mo Kα, λ = 0.71073 Å) with high-brilliance and high-performance focusing multilayer optics. Standard *APEXII* software was used for determination of the unit cells and data collection control. The intensities of the reflections of a sphere were collected by a combination of multiple sets of exposures (frames). Each set had a different φ angle for the crystal, and each exposure covered a range of 0.5° in ω. A total of 1464 images with an exposure time of 10−20 s were collected depending on the crystal. *SAINT* software was used for data integration including Lorentz and polarization corrections. Crystallographic data for all three compounds can be found in Table 1. Crystals of **$Pu^{IV}Mo$** were nonmerohedrally twinned with a rotation angle of 180°. The program *CELL_NOW* was used to index the twinned crystal. Multiscan absorption corrections were applied using the program *SADABS* or *TWINABS*.

UV−Vis−Near-IR (NIR) Spectroscopy. UV−vis−NIR data were acquired from single or twinned crystals using a Craic Technologies microspectrophotometer. Crystals were placed on quartz slides under immersion oil, and the data were collected from 200 to 1200 nm for **$Pu^{III}Mo$** and for **$Pu^{IV}Mo$**.

Table 1. Crystallographic Information for $Pu^{III}Mo$, $Pu^{IV}Mo$, and NdMo

compound	$Pu^{III}Mo$	$Pu^{IV}Mo$	$Nd^{III}Mo$
formula mass	497.85	1717.64	2576.24
color and habit	green, plate	orange, column	pink, cube
space group	$P2_1/c$	$C2/c$	$R\bar{3}c$
a (Å)	12.345(1)	12.687(2)	17.3669(3)
b (Å)	7.0820(8)	22.052(3)	17.3669(3)
c (Å)	7.2016(8)	7.806(1)	25.4356(5)
α (deg)	90	90	90
β (deg)	103.408(2)	96.683(3)	90
γ (deg)	90	90	120
V (Å^3)	612.4(1)	26169.0(5)	6643.8(3)
Z	4	4	6
T (K)	100	100	296
λ (Å)	0.71073	0.71073	0.71073
max 2θ (deg)	30.55	28.31	27.493
ρB_{calcd} (g cm^{-3})	5.399	5.260	3.863
μ(Mo Kα) (cm^{-1})	191.77	124.38	79.94
$R(F)$ for $F_o^2 > 2\sigma(F_o^2)^a$	0.0323	0.0334	0.0365
$R_w(F_o^2)^b$	0.0888	0.0637	0.1014

$^aR(F) = \sum||F_o| - |F_c||/\sum|F_o|$. $^bR_w(F_o^2) = [\sum[w(F_o^2 - F_c^2)^2]/\sum wF_o^4]^{1/2}$.

RESULTS AND DISCUSSION

Structure and Topological Description. **$Pu^{III}Mo$** crystallizes in the space group $P2_1/c$ and adopts a layered topology with slabs that propagate parallel to the *bc* plane. The slabs are composed of Pu^{3+} polyhedra and MoO_4^{2-} tetrahedra. The substructure consists of Pu^{3+} polyhedra on the outside with MoO_4^{2-} anions in the center of the layer. The Pu^{3+} polyhedra edge share, forming chains parallel to the *c* axis. These chains are linked together by the molybdate anions, as shown in Figure 1.

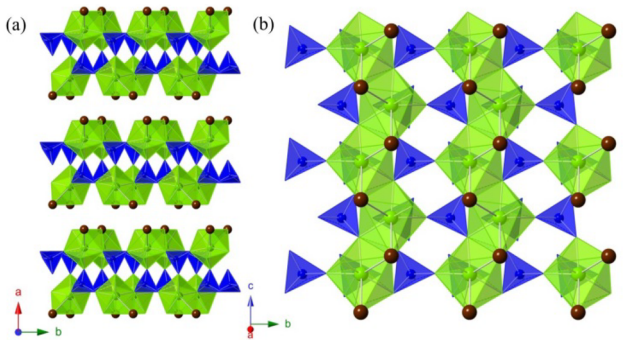

Figure 1. Polyhedral representations of **$Pu^{III}Mo$**. (a) View down the *c* axis showing the stacking of the layers. (b) Single layer of one of the sheets. Pu^{3+} is represented as green polyhedra, MoO_4^{2-} is represented as blue tetrahedra, and Br^- is represented as brown spheres.

The Pu^{3+} center is eight-coordinate with an approximate geometry of a bicapped trigonal prism.[7] The coordination environment is composed of five O atoms donated from molybdate, one coordinating water molecule, and two Br^- anions, as shown in Figure 2. The edge-sharing interaction is formed through Br^- and one of the O atoms donated from molybdate. Br^- and the water molecule make up the same face on the outer part of the slab, holding the slabs together through intermolecular forces.[8] The Pu−O bond distances range from 2.347(7) to 2.524(7) Å, and the Pu−Br distances are 3.042(1)

dx.doi.org/10.1021/ic403116r | Inorg. Chem. 2014, 53, 3148−3152

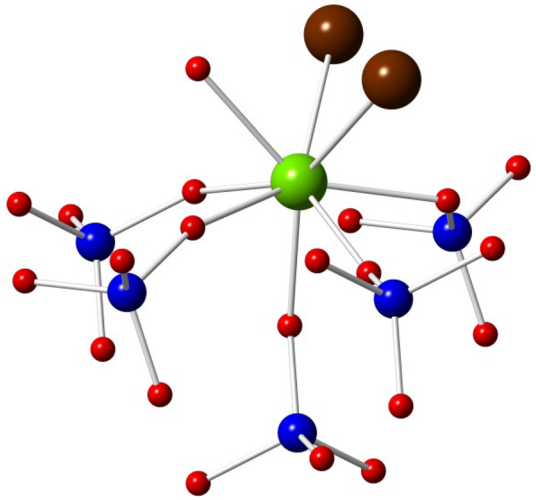

Figure 2. Coordination environment of Pu^{3+} in **$Pu^{III}Mo$**, with Pu^{3+} represented as a green sphere, Mo atoms represented as blue spheres, O atoms represented as red spheres, and Br atoms represented as brown spheres.

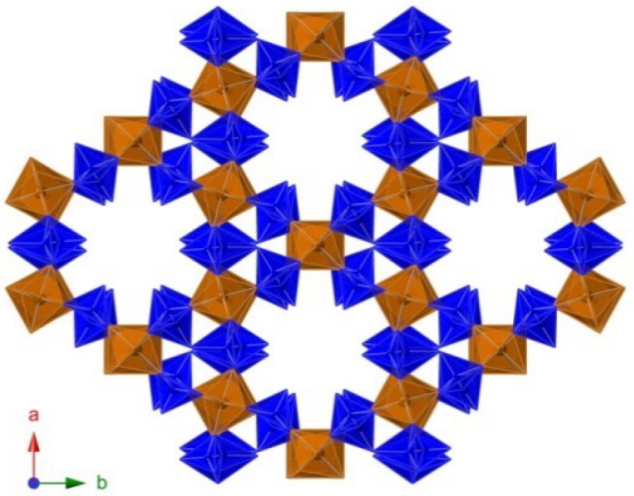

Figure 3. Polyhedral representation of **$Pu^{IV}Mo$** along the *c* axis showing the channels. Pu^{4+} sites are represented as orange polyhedra, and Mo^{6+} sites are represented as blue polyhedra.

and 3.069(1) Å. The molybdate forms a nearly ideal tetrahedron with four short Mo−O bonds with an average bond distance of 1.77(3) Å. Selected bond distances are given in Table 2.

Table 2. Selected Bond Distances for $Pu^{III}Mo$ and $Pu^{IV}Mo$

$Pu^{III}Mo$		$Pu^{IV}Mo$	
Pu(1)−O(5)	2.347(7)	Pu(1)−O(3)	2.221(6)
Pu(1)−O(2)	2.402(7)	Pu(1)−O(3)	2.221(6)
Pu(1)−O(4)	2.407(7)	Pu(1)−O(1)	2.275(6)
Pu(1)−O(2)	2.483(6)	Pu(1)−O(1)	2.275(6)
Pu(1)−O(3)	2.493(7)	Pu(1)−O(2)	2.296(6)
Pu(1)−O(1)	2.524(7)	Pu(1)−O(2)	2.296(6)
Pu(1)−Br(1)	3.042(1)	Pu(1)−O(1)	2.492(6)
Pu(1)−Br(1)	3.069(1)	Pu(1)−O(1)	2.492(6)
Pu(1)−Pu(1)	4.0887(5)	Pu(2)−O(6)	2.222(6)
Mo(1)−O(4)	1.744(7)	Pu(2)−O(9)	2.241(7)
Mo(1)−O(3)	1.745(7)	Pu(2)−O(8)	2.270(6)
Mo(1)−O(5)	1.756(7)	Pu(2)−O(7)	2.284(6)
Mo(1)−O(2)	1.817(6)	Pu(2)−O(4)	2.307(6)
		Pu(2)−O(5)	2.408(6)
		Pu(2)−O(5)	2.423(6)
		Pu(2)−O(7)	2.455(6)

No f-block molybdate bromides exist. A series of lanthanide molybdate chlorides have been synthesized, but their topologies do not match that of **$Pu^{III}Mo$**.[9] This is expected because most of these phases were made through typical solid-state reactions, not hydrothermally. The presence of Br^- in the inner coordination sphere of Pu^{3+} in competition with oxyanions is somewhat common and has been seen in both of the plutonium(III) borate bromides.[10]

$Pu^{IV}Mo$ crystallizes in the space group *C*2/*c* and is nearly isotypic to the previously reported $CsPu_3Mo_6O_{24}(H_2O)$ and $Ce_3Mo_6O_{24}(H_2O)_4$. This structure type is a channel structure built of disordered molybdate square pyramids and PuO_8 trigonal dodecahedra, as shown in Figure 3. **$Pu^{IV}Mo$** is more of a structural match for the cerium(IV) complex because there is no Cs^+ in the channel and no mixed valency. Unlike the cerium(IV) complex, no water was crystallographically resolved in the channels although electron density corresponding to approximately two water molecules was inferred using *SQUEEZE* from *PLATON*.[11] The water in the given formula arises as a consequence of the disordered molybdates. The structural topology will not be discussed further here because this structure was discussed at length earlier.[6] The Pu−O bond distances range from 2.221(6) to 2.492(6) Å, in line with the previously reported bond distances, and are given in Table 2.

$Nd^{III}Mo$ crystallizes in the space group $R\bar{3}c$ and is a dense three-dimensional (3D) network. This structure is isotypic to a previously reported gadolinium complex.[12] The framework is built from Silverton-type anions of $[NdMo_{12}O_{42}]^{9-}$ that are charge-balanced and interconnected by Nd^{3+} cations, forming the 3D framework, as shown in Figure 4.[13] The Nd^{3+} centered in the Silverton-type cluster is a 12-coordinate icosahedron, where all O atoms are donated from molybdate with an average bond distance of 2.54(8) Å. The Nd^{3+} outside the cluster is 9-coordinate with an approximate geometry of a tricapped trigonal prism, where three O atoms are coordinating water molecules and six O atoms are donated from molybdate anions. The two crystallographically independent Mo atoms are both distorted octahedra with two short (∼1.70 Å), two intermediate (∼1.90 Å), and two long (∼2.2 Å) Mo−O bonds. Selected bond distances for **$Nd^{III}Mo$** are given in Table 3.

UV−Vis−NIR Spectroscopy. Absorption data were collected for both plutonium compounds on crystals using a microspectrophotometer. The f−f transitions of the actinides are diagnostic of their oxidation state and tend to shift very little with the coordination environment; this is especially true with hard oxoanion donors.[14] The assignment of the trivalent state for **$Pu^{III}Mo$** is confirmed by the signature peak at approximately 910 nm, as shown in Figure 5a. This transition is typically centered around 900 nm; however, upon close inspection, all of the f−f transitions are red-shifted by approximately 10 nm compared to those of previously reported spectra.[2a,3,10]

The f−f transitions in Pu^{4+} are more complicated than those in Pu^{3+}, and the higher-energy transitions arise from multiple *J* states. The peak positions can still be used for oxidation state assignment. However, in the case of **$Pu^{IV}Mo$**, this is not

dx.doi.org/10.1021/ic403116r | *Inorg. Chem.* 2014, 53, 3148−3152

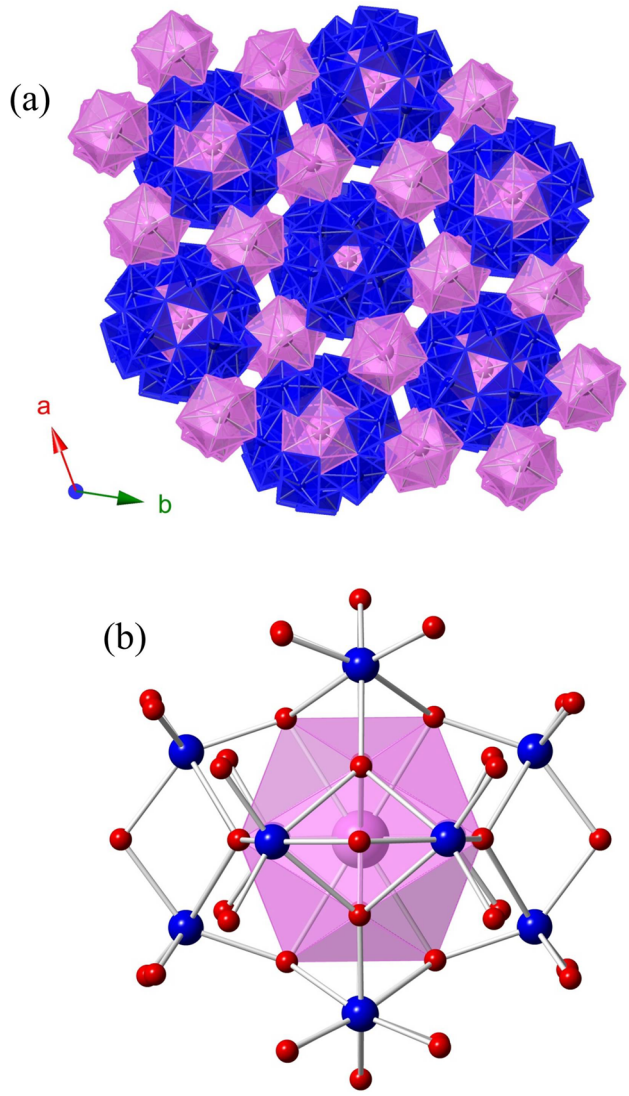

Figure 4. (a) Polyhedral view of **Nd^{III}Mo** parallel to the *c* axis showing Silverton-type clusters connected by Nd^{3+} cations outside the cluster. (b) Coordination sphere of the clusters showing the icosahedral geometry of Nd^{3+}. Nd is represented in pink, Mo is represented in blue, and O is represented in red.

straightforward because all of the transitions have been shifted by ~20 nm compared to plutonium(IV) phosphite and phosphonate. When this shift is taken into account, the spectrum matches that of Pu^{4+}, as shown in Figure 5b.

A shift in the f−f transitions can be attributed to either enhanced covalency in the complex or strong crystal-field effects and is commonly seen with soft donors. For instance, the alkylated BTP complex with plutonium(III) produced a shift of 36 nm.[15] Red shifts with oxyanion complexes are much less common, especially with inorganic oxygen donors. Without more analysis, it is impossible to distinguish the factor that brings about the shift seen in these compounds.

Both complexes also exhibit broad charge-transfer (CT) peaks. The Pu^{3+} band extends from ~300 to 500 nm, with the Pu^{4+} band being approximately 50 nm narrower, extending from ~300 to 450 nm.[16] The ligand-to-metal charge transfer (LMCT) of d^0 complexes is well-known because the ligand donates electron density to compensate for the electron deficiency at the metal site. In these complexes, the LMCT

Table 3. Selected Bond Distances for Nd^{III}Mo

Nd(1)−O(2)	2.419(6)	Mo(1)−O(3)	1.713(6)
Nd(1)−O(2)	2.419(6)	Mo(1)−O(4)	1.729(6)
Nd(1)−O(9)	2.45(1)	Mo(1)−O(1)	1.870(6)
Nd(1)−O(3)	2.495(6)	Mo(1)−O(5)	1.954(6)
Nd(1)−O(3)	2.496(6)	Mo(1)−O(1)	2.251(5)
Nd(1)−O(4)	2.516(6)	Mo(1)−O(6)	2.265(6)
Nd(1)−O(4)	2.516(6)	Mo(2)−O(7)	1.700(6)
Nd(1)−O(8)	2.550(8)	Mo(2)−O(2)	1.726(6)
Nd(1)−O(8)	2.550(8)	Mo(2)−O(6)	1.906(6)
Nd(2)−O(1)	2.537(6)	Mo(2)−O(5)	1.958(6)
Nd(2)−O(1)	2.537(6)	Mo(2)−O(6)	2.222(6)
Nd(2)−O(1)	2.537(6)	Mo(2)−O(1)	2.300(5)
Nd(2)−O(1)	2.537(6)		
Nd(2)−O(1)	2.537(6)		
Nd(2)−O(1)	2.537(6)		
Nd(2)−O(6)	2.552(6)		
Nd(2)−O(6)	2.552(6)		
Nd(2)−O(6)	2.552(6)		
Nd(2)−O(6)	2.552(6)		
Nd(2)−O(6)	2.552(6)		
Nd(2)−O(6)	2.552(6)		

of molybdate is coupled with the metal-to-ligand charge transfer (MLCT) of Pu^{3+} and Pu^{4+}, producing broad absorption bands. Pu^{4+} should have a smaller MLCT than Pu^{3+} because the higher charge decreases the propensity of electron removal, resulting in smaller absorption band. This suggests that there is enough orbital overlap that at higher energies electrons are being promoted from f metal to ligand and then from ligand to d metal, a coupling of the charge donator and charge acceptor.

CONCLUSION

Further explorations in the f-element molybdate system have provided some noteworthy results. The hydrothermal reaction of $PuBr_3$ or $NdBr_3$ with MoO_3 at 200 °C produces drastically different compounds. It is unclear if covalent effects from plutonium(III) drives this structural discrepancy or if there are some other influencing factors. The spectrum of **Pu^{III}Mo** features a broad CT band, suggesting significant CT from molybdate and a propensity to be oxidized. This propensity is confirmed by isolating **Pu^{IV}Mo** by simply increasing the reaction temperature of 30 °C while keeping the reaction in an inert atmosphere. The electronic absorption spectra are also unusual in that both complexes have broad CT bands and significant red shifts that are not typically seen in 5f complexes with oxoanions. The combination of a d^0 metal with low-valent plutonium seems to produce the CT observed through a coupling of the LMCT of molybdate and the MLCT of plutonium. Because cerium(III) has an easily accessible tetravalent state, it may be possible to see broad CTs in lanthanide complexes as well. Changing the d^0 metal could have drastic changes in the electronic character of these complexes as the frontier orbitals shift in energy. The transplutonium elements also need to be explored in this system because it is unclear how they will behave structurally and electronically and will provide insight into whether the unusual electronic characteristics are due to bonding or redox instability.

dx.doi.org/10.1021/ic403116r | *Inorg. Chem.* 2014, 53, 3148−3152

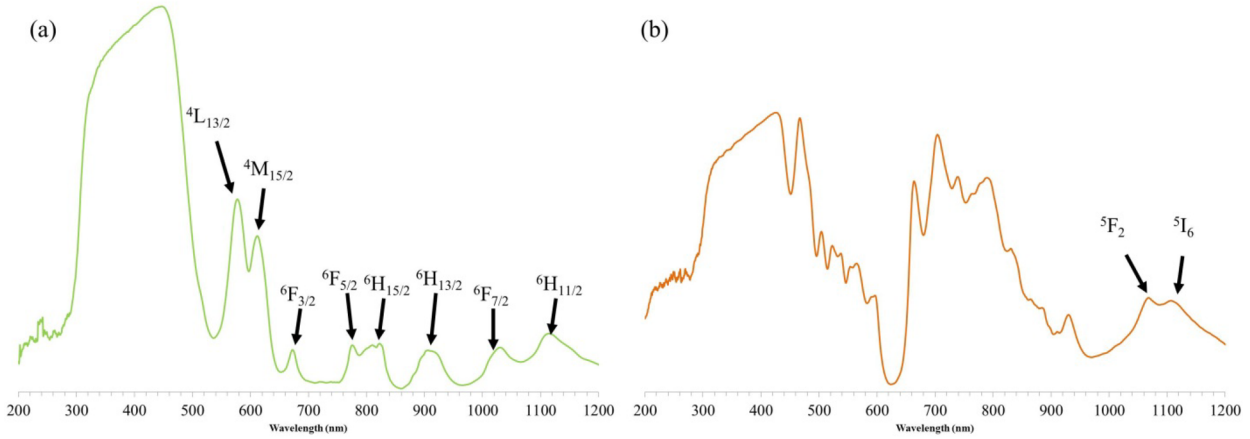

Figure 5. Absorption spectra of $\mathbf{Pu^{III}Mo}$ (a) and $Pu_3Mo_6O_{24}(H_2O)$ (b). (a) Diagnostic peaks at 580, 620, and 900 nm confirm the 3+ oxidation state. The large CT band is unusual in plutonium(III) complexes and accounts for the green color of the crystals as the compound absorbs well into the blue region. All transitions are from labeled as the excited state returning to the ground state of $^6H_{5/2}$. (b) Diagnostic peaks of plutonium(IV) centered around 1100 nm are labeled. The CT band is ~50 nm narrower than that of the CT band in the plutonium(III) complex. The labeled transitions are relaxations to the ground state.

■ ASSOCIATED CONTENT

Supporting Information

Additional structural views, photographs of crystals, and a CIF file. This material is available free of charge via the Internet at http://pubs.acs.org.

■ AUTHOR INFORMATION

Corresponding Author

*E-mail: talbrecht-schmitt@chem.fsu.edu.

Notes

The authors declare no competing financial interest.

■ ACKNOWLEDGMENTS

We are grateful for support provided by the Materials Science of Actinides, an Energy Frontier Research Center funded by the U.S. Department of Energy, Office of Science, Office of Basic Energy Sciences, under Award DE-SC0001089.

■ REFERENCES

(1) (a) Neidig, M. L.; Clark, D. L.; Martin, R. L. *Coord. Chem. Rev.* **2013**, *257*, 394. (b) Wen, X.-D.; Martin, R. L.; Henderson, T. M.; Scuseria, G. E. *Chem. Rev.* **2013**, *113* (2), 1063. (c) Edelstein, N. A.; Lander, G. H. Magnetic Properties. In *The Chemistry of the Actinides and Transactinide Elements*, 4th ed.; Morss, L. R., Edelstein, N. A., Fuger, J., Katz, J. J., Eds.; Springer: Dordrecht, The Netherlands, 2011; Vol. 4, p 2225.

(2) (a) Polinski, M. J.; Grant, D. J.; Wang, S.; Alekseev, E. V.; Cross, J. N.; Villa, E. M.; Depmeier, W.; Gagliardi, L.; Albrecht-Schmitt, T. E. *J. Am. Chem. Soc.* **2012**, *134*, 10682. (b) Gaunt, A. J.; Scott, B. L.; Neu, M. P. *Angew. Chem., Int. Ed.* **2006**, *45*, 1638. (c) Gaunt, A. J.; Reilly, S. D.; Enriquez, A. E.; Scott, B. L.; Ibers, J. A.; Sekar, P.; Ingram, K. I. M.; Kaltsoyannis, N.; Neu, M. P. *Inorg. Chem.* **2008**, *47*, 29. (d) Kozimor, S. A.; Yang, P.; Batista, E. R.; Boland, K. S.; Burns, C. J.; Clark, D. L.; Conradson, S. D.; Martin, R. L.; Wilkerson, M. P.; Wolfsberg, L. E. *J. Am. Chem. Soc.* **2009**, *131*, 12125.

(3) (a) Apostolidis, C.; Schimmelpfennig, B.; Magnani, N.; Lindqvist-Reis, P.; Walter, O.; Sykora, R.; Morgenstern, A.; Colineau, E.; Caciuffo, R.; Klenze, R.; Haire, R. G.; Rebizant, J.; Bruchertseifer, F.; Fanghanel, T. *Angew. Chem., Int. Ed.* **2010**, *49*, 343. (b) Cross, J. N.; Villa, E. M.; Wang, S.; Diwu, J.; Polinski, M. J.; Albrecht-Schmitt, T. E. *Inorg. Chem.* **2012**, *51*, 8419. (c) Diwu, J.; Grant, D. J.; Wang, S.; Gagliardi, L.; Albrecht-Schmitt, T. E. *Inorg. Chem.* **2012**, *51*, 6906.

(4) Goodey, J.; Broussard, J.; Halasyamani, P. S. *Chem. Mater.* **2002**, *14*, 3174.

(5) (a) Lin, J.; Diwu, J.; Cross, J. N.; Villa, E. M.; Albrecht-Schmitt, T. E. *Inorg. Chem.* **2012**, *51*, 1008. (b) Lin, J.; Cross, J. N.; Diwu, J.; Meredith, N. A.; Albrecht-Schmitt, T. E. *Inorg. Chem.* **2013**, *52*, 4277.

(6) Cross, J. N.; Duncan, P. M.; Villa, E. M.; Polinski, M. J.; Babo, J.-M.; Alekseev, E. V.; Booth, C. H.; Albrecht-Schmitt, T. E. *J. Am. Chem. Soc.* **2013**, *135*, 2769.

(7) Xu, J.; Radkov, E.; Ziegler, M.; Raymond, K. N. *Inorg. Chem.* **2000**, *39*, 4156–4164.

(8) Alvarez, S. *Dalton Trans.* **2013**, *42*, 8617.

(9) (a) Hartenbach, I.; Strobel, S.; Schleid, T.; Kramer, K. W.; Dorhout, P. K. *Z. Anorg. Allg. Chem.* **2009**, *635*, 966. (b) Schleid, T.; Hartenbach, I. *Z. Anorg. Allg. Chem.* **2009**, *635*, 1904. (c) Hartenbach, I.; Strobel, S.; Schleid, T.; Dorhout, P. K. *Z. Anorg. Allg. Chem.* **2010**, *636*, 1183.

(10) (a) Wang, S.; Alekseev, E. V.; Depmeier, W.; Albrecht-Schmitt, T. E. *Inorg. Chem.* **2011**, *50*, 2079. (b) Polinski, M. J.; Wang, S.; Cross, J. N.; Alekseev, E. V.; Depmeier, W.; Albrecht-Schmitt, T. E. *Inorg. Chem.* **2012**, *51*, 7859.

(11) Spek, A. L. *J. Appl. Crystallogr.* **2003**, *36*, 7.

(12) Wu, C.-D.; Lu, C.-Z.; Zhuang, H.-H.; Huang, J.-S. *J. Am. Chem. Soc.* **2002**, *124*, 3836.

(13) Dexter, D. D.; Silverton, J. V. *J. Am. Chem. Soc.* **1968**, *90*, 3589.

(14) (a) Pappalardo, R. G.; Carnall, W. T.; Fields, P. R. *J. Chem. Phys.* **1970**, *53*, 2922. (b) Carnall, W. T.; Liu, G. K.; Williams, C. W.; Reid, M. F. *J. Chem. Phys.* **1991**, *95*, 7194. (c) Banik, N. L.; Schimmelpfennig, B.; Marquardt, C. M.; Brendebach, B.; Geist, A.; Denecke, M. A. *Dalton Trans.* **2010**, *39*, 5117.

(15) (a) Pappalardo, R. G.; Carnall, W. T.; Fields, P. R. *J. Chem. Phys.* **1969**, *51*, 842. (b) Liu, G. K.; Beitz, J. V. Optical Spectra and Electronic Structure. In *The Chemistry of the Actinides and Transactinide Elements*, 4th ed.; Morss, L. R., Edelstein, N. A., Fuger, J., Katz, J. J., Eds.; Springer: Dordrecht, The Netherlands, 2011; Vol. 3, p 2013.

(16) The unusual band shape is likely due to a combination of baseline drift and reaching the limits of the detector.